Journal of
Composites Science

MDPI

Article

A Comprehensive Study of Structural, Thermal, and Dielectric Properties of Melt-Processed Polypropylene/ $Ni_{0.9}Zn_{0.1}Fe_2O_4$ Nanocomposites

Taha Abdel Mohaymen Taha [1,2,*], Mohamed Tharwat [2] and Ali Ismael [3,*]

[1] Physics Department, College of Science, Jouf University, Skaka P.O. Box 2014, Saudi Arabia
[2] Physics and Engineering Mathematics Department, Faculty of Electronic Engineering, Menoufia University, Menouf 32952, Egypt; mohamed.attia@el-eng.menofia.edu.eg
[3] Physics Department, Lancaster University, Lancaster LA1 4YB, UK
* Correspondence: themaida@ju.edu.sa (T.A.M.T.); k.ismael@lancaster.ac.uk (A.I.)

Abstract: This article explores the processing of structural, thermal, and dielectric properties of polypropylene (PP) polymer nanocomposites modified with $Ni_{0.9}Zn_{0.1}Fe_2O_4$. The PP/$Ni_{0.9}Zn_{0.1}Fe_2O_4$ nanocomposites are manufactured by the melt-processing method using a Brabender Polyspeed B. The XRD and FTIR structural investigations assure good incorporation of $Ni_{0.9}Zn_{0.1}Fe_2O_4$ into the PP matrix. It should be noted that adding $Ni_{0.9}Zn_{0.1}Fe_2O_4$ NPs to the PP polymer matrix enhances the polymer's thermal stability. Utilizing the Coats–Redfern model, kinetic thermodynamic parameters such as activation energy (Ea), enthalpy (ΔH), entropy (ΔS), and Gibbs free energy (ΔG*) are deduced from TGA data. The dielectric results showed an increase in ε' with the introduction of nanoparticles into the PP matrix. As the content of $Ni_{0.9}Zn_{0.1}Fe_2O_4$ NPs in these nanocomposite films increases, the loss tangent values decrease at higher frequencies while increasing at lower frequencies. The estimated ε_s and ε_∞ of PP nanocomposites using Cole–Cole plots reveal an improvement when NPs are added to PP. We believe that the proposed work suggests a relevant step towards the practical application of PP/$Ni_{0.9}Zn_{0.1}Fe_2O_4$ nanocomposites.

Keywords: $Ni_{0.9}Zn_{0.1}Fe_2O_4$; polypropylene nanocomposite; TGA kinetics; dielectric constant

Citation: Taha, T.A.M.; Tharwat, M.; Ismael, A. A Comprehensive Study of Structural, Thermal, and Dielectric Properties of Melt-Processed Polypropylene/$Ni_{0.9}Zn_{0.1}Fe_2O_4$ Nanocomposites. *J. Compos. Sci.* **2024**, *8*, 117. https://doi.org/10.3390/jcs8040117

Academic Editor: Kyong Yop Rhee

Received: 10 February 2024
Revised: 9 March 2024
Accepted: 18 March 2024
Published: 22 March 2024

1. Introduction

The thermal, mechanical, and electrical properties of polymer nanocomposites have generated great interest in academic research [1–4]. Polymer nanocomposites can have enhanced thermal stability, improved heat resistance, and higher thermal conductivity. The thermal conductivity of polymer nanocomposites can be increased by the addition of nanoparticles with high thermal conductivity, such as graphene, carbon nanotubes, or metal particles. Surprisingly, even small amounts of nanofillers can revolutionize the properties of polymer composites compared to pure polymer [5–9]. Therefore, polymer nanocomposites have found wide application in many fields, including electromagnetic shielding, charge storage capacitors, microwave absorbers [10–12], EM detectors [13], optical integrated circuits, sensors, medical devices, aerospace, packaging materials, consumer goods, and so on [14]. Various scientific methodologies can be used to adapt the physical properties of polymeric nanomaterials for a specific application. The physical and chemical properties of polymer nanocomposites are related to the shape, size, and content of the nanoparticles [15–24]. Since it offers amazing properties that can be used in catalysis, biomedicine, high-density information storage devices, transformer cores, electromagnetic interference (EMI) suppressors, rod antennas, gas detecting, and environmental remediation, nano-ferrite is subject to substantial research [25–29].

Polypropylene (PP) is readily available and cost-effective from refineries across the world. Its low density makes it easy to process using melt-processing methods [30–33].

Furthermore, its high chemical resistance makes PP ideal for packaging, automobiles, and other applications [34–36]. Therefore, scientists have been actively studying polypropylene nanocomposites to enhance the physical properties of pure PP [35,37–54]. There are research works related to the preparation and investigation of thermal and dielectric properties of polypropylene nanocomposites. This is an active area of research with great potential for developing new materials with improved properties. Siddiqui et al. [40] successfully manufactured new magnetic bionanocomposites of graphene bonded to magnetically modified polypropylene (as the polymer matrix). The overall conductivity of the composites was significantly improved. Rheological experiments demonstrated that increasing the nanofiller concentration led to an enhancement of viscoelastic characteristics, exhibiting more solid-like behavior. The dispersion of the nanofillers within the PP matrix created conductive connections, resulting in innovative PP/MCNC composites with an 800% increase in shielding efficiency compared to pure PP. Bendaoued et al. [43] demonstrated that nanofillers were synthesized using the sol-gel process and incorporated as fillers in polypropylene composites to enhance the thermal, rheological, and interfacial compatibility of the final material. The addition of nano-TiO_2 improved the thermal degradation stability of polypropylene. The results revealed that incorporating nano-TiO_2 into the polypropylene matrix increased the degree of crystallinity. Due to its superior thermal and viscoelastic properties, including high storage and loss moduli and degree of crystallinity, the nanocomposite PP@5% TiO_2 is a suitable candidate for application in the manufacture of recycled wind turbine blades. Rishaban et al. [42] referred to the significantly improved mechanical and thermal stability of the created polymer/multi-layered graphene nanocomposites. P. Tambe et al. [32] demonstrated that the NaOH-treated halloysite nanotubes (H.N.Ts) are superior fillers for reinforcing the PP matrix. This modification is cost-effective for the industry because NaOH is available in large quantities at a lower cost than other synthetic organic modifiers. In comparison to clean PP and H.N.Ts-filled PP nanocomposites, the mechanical characteristics enhancement is greatest for the 3 wt.% NaOH-treated H.N.Ts-filled PP nanocomposites. Uo Uyor et al. [39] studied the mechanical, thermal, and dielectric properties of sandwich-structured BN-$BaTiO_3$-BN/PP nanocomposites. Hydrothermal and assembly processes were used to create the BN-$BaTiO_3$-BN sandwich nanoparticles. A rheometer prepared the nanocomposites using the melt compounding process. The prepared PP nanocomposites exhibited improved thermal properties above 20 °C. Additionally, the dielectric constant increased by nearly 132%, from 2.02 at 100 Hz for pure PP to 4.68 for PP/5BN-15BT nanocomposite. Moreover, the nanocomposite maintained a low loss of approximately 0.05 at 100 Hz. L.G. Furlan et al. [38] discussed the role of processing conditions on the thermal and mechanical properties of PP nanocomposites. Using a co-rotating twin-screw extruder, polypropylene montmorillonite (PP-MMT) nanocomposites were fabricated. Their findings demonstrated that a medium shear intensity profile, as opposed to a high one, produced a greater improvement in mechanical properties. The dispersion and interaction of MMT particles within the PP matrix influenced the reinforcement effect. Patil et al. [35] studied the mechanical and thermal properties of polypropylene (PP)/multiwall carbon nanotubes (MWCNTs) nanocomposites. They fabricated the nanocomposites using compression molding equipment. The mechanical and thermal behavior of the nanocomposites was then evaluated using ASTM standards. The results revealed that adding MWCNTs to the PP matrix enhanced both mechanical and thermal properties. The highest tensile strength (62.80%) was measured at 1.2 wt.% MWCNT loading. At 1.5 wt.%, impact strength and hardness increased by 82.14% and 12.44%, respectively. However, low weight percent increases were accompanied by subsequent drops in glass transition temperature.

The addition of $Ni_{0.9}Zn_{0.1}Fe_2O_4$ nanoparticles as a nanofiller to a polypropylene (PP) polymer matrix can have significant impacts on the structure, thermal, and dielectric properties of the resulting composite material. $Ni_{0.9}Zn_{0.1}Fe_2O_4$ nanoparticles exhibit ferrimagnetic behavior [55], possess high thermal stability [56], and have higher dielectric constants [57] compared to the polymer matrix. Therefore, the introduction of $Ni_{0.9}Zn_{0.1}Fe_2O_4$ nanoparticles can improve the thermal stability and dielectric constant of the composite.

The mechanisms by which nanoparticles influence the thermal and dielectric properties of polymers are still not fully understood. Further research is needed to elucidate these mechanisms, which will enable the rational design of nanocomposites with desired properties. Therefore, in current research, PP/$Ni_{0.9}Zn_{0.1}Fe_2O_4$ nanocomposites were synthesized using the melt-processing method. The aim of this research is to investigate the effect of adding $Ni_{0.9}Zn_{0.1}Fe_2O_4$ nanoparticles (NPs) to the PP matrix on the structural, thermal, and dielectric properties. XRD and FTIR analysis to confirm the dispersion and interaction between the NPs and the polymer. The addition of NPs has improved the thermal resistance of the polymer, potentially leading to applications in high-temperature environments. Using TGA data and the Coats–Redfern model, the activation energy, enthalpy, entropy, and Gibbs free energy associated with the thermal degradation process were determined. The introduction of NPs influences the dielectric constant (ε′) and loss tangent of the material. By analyzing the Cole–Cole plots, the static and high-frequency permittivities (ε_s and ε_∞) of the nanocomposites were estimated, potentially leading to advancements in electrical insulation or dielectric materials.

2. Materials and Methods

2.1. Materials

Ferric nitrate AR ($Fe(NO_3)_3 \cdot 9H_2O$, M.W 404, ALPHA CHEMIKA, Maharashtra, India 99%), nickel nitrate AR ($Ni(NO_3)_2 \cdot 6H_2O$, M.W 290.8, Nile Company, Cairo, Egypt, 99%), zinc nitrate AR ($Zn(NO_3)_2 \cdot {}_6H_2O$, M.W 297.49, Cairo, Egypt, 99%), commercial bovine gelatin (Foodkum, Cairo, Egypt), and polypropylene raw material PPR-MS16 (GM1600E, SINOPEC, Beijing, China) were used for the preparation of PP/$Ni_{0.9}Zn_{0.1}Fe_2O_4$ nanocomposites.

2.2. Sample Preparation and Characterization Techniques

According to Reference [58], $Ni_{0.9}Zn_{0.1}Fe_2O_4$ nanoparticles were synthesized using the green sol-gel autocombustion process. Nanocomposites composed of PP and $Ni_{0.9}Zn_{0.1}Fe_2O_4$ nanoparticles were then successfully fabricated via the melt-processing technique. The ratios of $Ni_{0.9}Zn_{0.1}Fe_2O_4$ were 0.0, 5.0, 10, and 15 wt%, as shown in Table 1. The PP and nanoparticles were pre-dried to remove any moisture that could affect the processing and final properties of the nanocomposite. A Brabender Polyspeed B was the specific type of internal mixer used to mix the molten polymer with the nanoparticles under controlled temperature and pressure. After mixing, the molten mixture was shaped into disk shapes using a compression molding technique. The nanocomposites were stored in a desiccator to minimize moisture absorption before characterization.

Table 1. Composition of polypropylene nanocomposites.

Sample ID	Polypropylene (wt%)	$Ni_{0.9}Zn_{0.1}Fe_2O_4$ (wt%)
PP	100	0.0
PP-NZF5	95	5.0
PP-NZF10	90	10
PP-NZF15	85	15

Structural analyses of the prepared nanocomposites were conducted using a Bruker AXS D8 Advance diffractometer (Berlin, Germany) equipped with CuKα radiation (λ = 0.154060 nm) and a collimator size of 480 μm. A high-performance FE-SEM Quanta FEG 250 provided high-resolution imaging and analysis of the polymer nanocomposite morphology. High-resolution imaging of materials and particle size at the nanoscale was achieved using a JEM-2100 instrument (JEOL Ltd., Tokyo, Japan). Functional group identification, molecular composition determination, and investigation of chemical bonding within the polymer nanocomposites were performed using a JASCO FT/IR-6100 (JASCO, Tokyo, Japan) spectrometer. Thermogravimetric analysis (TGA) of a polymer nanocomposite was conducted using an SDT Q600 TGA/DSC (TA Instruments, New Castle, DE, USA) analyzer with a heating rate of 10 °C/min. The dielectric properties of the polymer nanocomposites

were recorded over a wide frequency range (20 Hz–2.0 MHz) using a Keysight E4980 LCR meter (Octopart, New York, NY, USA). The thickness of the composite samples was 2.0 mm. The electrodes were coated with gold and had an across-section area of 3.14 cm^2. The samples were pre-dried to remove moisture prior to dielectric properties measurements.

3. Results

3.1. XRD Analysis

Figure 1 demonstrates the XRD spectra of polypropylene doped with $Ni_{0.9}Zn_{0.1}Fe_2O_4$ nanoparticles at different weight ratios: 0.0, 5.0, 10, and 15 wt%. The diffraction pattern of PP exhibits characteristic peaks at 14.11°, 16.78°, 18.47°, 19.84°, 21.10°, 21.84°, and 25.21°, corresponding to the lattice planes of the monoclinic crystals of (110), (040), (130), (111), (131), (060), and (220), respectively [44,59–62]. The XRD patterns of PP/$Ni_{0.9}Zn_{0.1}Fe_2O_4$ nanocomposites reveal the predominant peaks of PP along with additional peaks at 36°, 43°, 57.26°, and 62.90°, indicating the presence of $Ni_{0.9}Zn_{0.1}Fe_2O_4$ nanoparticles within the nanocomposites and confirming the formation of PP/$Ni_{0.9}Zn_{0.1}Fe_2O_4$ nanocomposite films [63,64]. Furthermore, the shift of major $Ni_{0.9}Zn_{0.1}Fe_2O_4$ nanoparticle peaks in the nanocomposite diffraction patterns towards lower angles due to crystal lattice changes confirms the successful formation of PP nanocomposites. $Ni_{0.9}Zn_{0.1}Fe_2O_4$ nanoparticles in polypropylene matrix induce strain in the lattice due to a mismatch in thermal expansion or processing stresses. This strain disrupts atomic arrangement, increasing interplanar spacing and shifting diffraction peaks to lower angles. Moreover, as the concentration of nanoparticles increases in the nanocomposite, the probability of interaction and stress transfer between the nanoparticles and the polymer matrix also increases. This can lead to a more pronounced lattice strain in the nanoparticles, resulting in a larger peak shift at higher weight percentages [65]. Some of the major peaks are indexed with Miller indices, as shown in the figure.

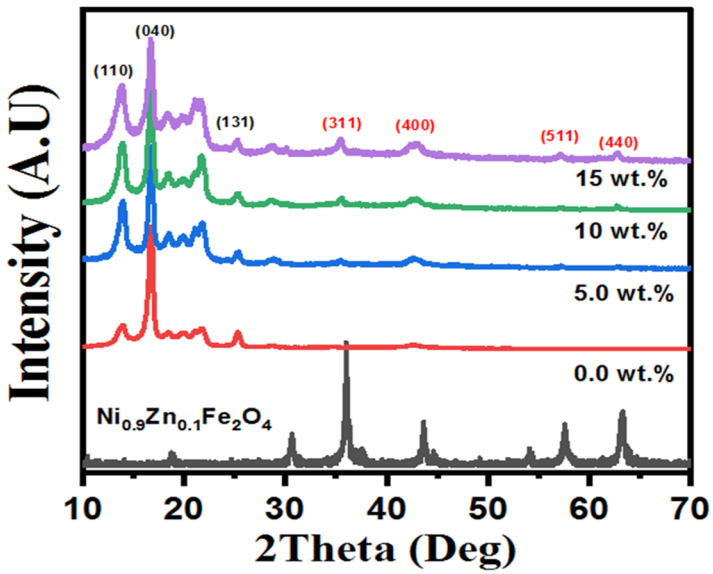

Figure 1. XRD patterns of PP/$Ni_{0.9}Zn_{0.1}Fe_2O_4$ nanocomposites films.

XRD peak broadening in PP/$Ni_{0.9}Zn_{0.1}Fe_2O_4$ polymer nanocomposites can be attributed to several factors related to the size and strain of the crystalline phases, as well as the presence of multiple phases. According to the Scherrer equation, smaller crystallites diffract X-rays less efficiently, leading to broader peaks in the XRD pattern. This broadening effect becomes more pronounced as the crystallite size in both the PP matrix and the $Ni_{0.9}Zn_{0.1}Fe_2O_4$ nanofillers decreases. Strain within the crystal lattice caused by imperfections, dislocations, or interfacial stresses between the PP and $Ni_{0.9}Zn_{0.1}Fe_2O_4$ phases can also broaden the XRD peaks. The presence of non-uniform phases or mixed

phases within the nanocomposite can contribute to peak broadening. This can arise from incomplete mixing of the PP and $Ni_{0.9}Zn_{0.1}Fe_2O_4$ components [66].

3.2. FTIR Analysis

One of the suitable techniques for studying such changes in these nanocomposite films is FTIR spectroscopy. Figure 2 illustrates the corresponding FTIR spectra within the range of 4000–400 cm^{-1} wavenumber for PP and its nanocomposites modified with different ratios of 5, 10, and 15 wt% $Ni_{0.9}Zn_{0.1}Fe_2O_4$ NPs. All spectra were quite similar, with each displaying the characteristic peaks of PP [44,67–69]. In the spectrum of PP, the vibrations of asymmetric CH_3, asymmetric CH_2, stretching CH_3, symmetric bending CH_3, rocking CH_3 or wagging CH, rocking CH_3 or stretching C-C, rocking CH_3 or rocking CH, and stretching C-C were attributed to the peak locations detected at wavenumbers of 2949, 2916, 2867, 1454–1375, 1165, 997, 972, 840, and 807 cm^{-1}, respectively [67].

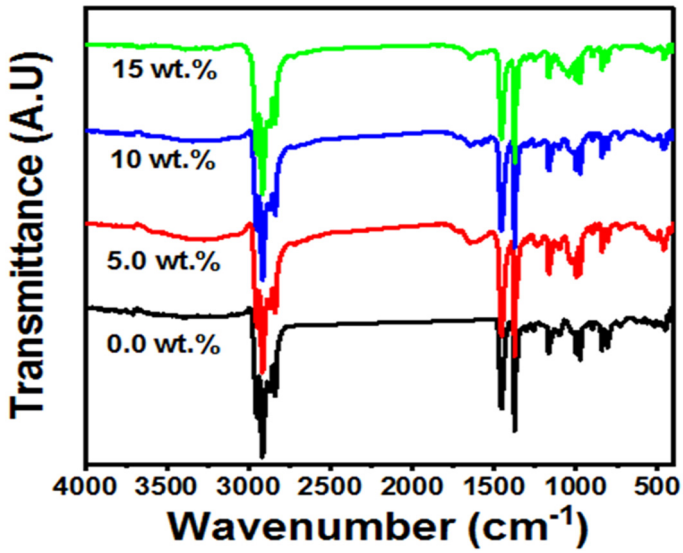

Figure 2. FTIR spectra of PP/$Ni_{0.9}Zn_{0.1}Fe_2O_4$ nanocomposite films.

In the spectra of PP nanocomposites, additional peaks appear at wavenumbers of 1645 and 460 cm^{-1}, which were assigned to the N-H band and octahedral complexes of the spinel cubic structure, respectively [58,63]. These extra peaks, observed in the nanocomposites, confirm the incorporation of $Ni_{0.9}Zn_{0.1}Fe_2O_4$ NPs in the PP matrix, in agreement with the XRD results. The peak at 1645 cm^{-1} is assigned to the N-H stretching vibration of adsorbed amine groups on the polypropylene matrix interacting with the Ni sites in the spinel. This suggests that there is a chemical bonding interaction between the amine groups on the polypropylene and the Ni atoms in the NPs. This type of interaction can lead to improved compatibility and dispersion of the NPs within the matrix, enhancing the mechanical and physical properties of the composite material. The peak at 460 cm^{-1} is assigned to the Fe-O vibrations in the octahedral sites of the spinel structure. The presence of Zn dopant ions can potentially affect these vibrations, leading to a shift in the peak position or intensity. This suggests that the Zn dopant ions may be influencing the local bonding environment around the Fe atoms in the NPs. This could, in turn, affect the interaction between the NPs and the polypropylene matrix.

3.3. TEM Microscopy

TEM image and electron diffraction of a selected area of $Ni_{0.9}Zn_{0.1}Fe_2O_4$ NPs are shown in Figure 3. As shown in the figure, nanoparticles have a spherical shape with an average crystal size of 29 nm, and some appear as dark regions due to the agglomeration of nanoparticles. Agglomeration is caused by the magneto-static interaction between particles.

Furthermore, the agglomeration phenomenon can be explained as nanoparticles having a permanent magnetic moment, which is directly proportional to their volume [58,70].

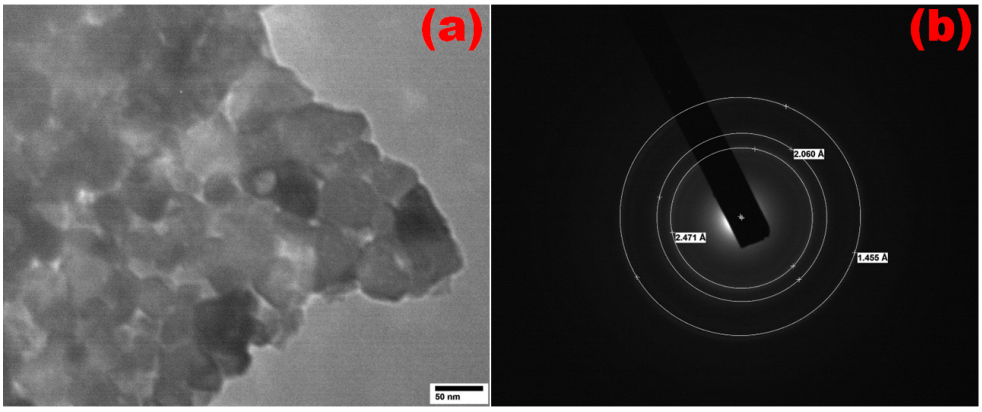

Figure 3. Images of (**a**) HRTEM and (**b**) electron diffraction of selected area for $Ni_{0.9}Zn_{0.1}Fe_2O_4$ NPs.

We compared the information obtained from electron diffraction (Figure 3b) with the bulk crystallographic data obtained from XRD. This showed a confirmation of the crystal structure obtained from XRD.

3.4. FESEM Microscopy

Figure 4 illustrates the FESEM images of PP/$Ni_{0.9}Zn_{0.1}Fe_2O_4$ nanocomposite films to investigate the morphology of the nanocomposites. The FESEM micrographs show a good distribution of $Ni_{0.9}Zn_{0.1}Fe_2O_4$ nanoparticles within the PP matrix, although some agglomeration is present. The appearance of agglomeration in the FE-SEM results (yellow circles) agrees well with the TEM results shown in Figure 3a. This suggests a good interaction between the $Ni_{0.9}Zn_{0.1}Fe_2O_4$ and the PP polymer matrix, confirming the formation of nanocomposites. This finding is consistent with the XRD and FTIR results [63,64].

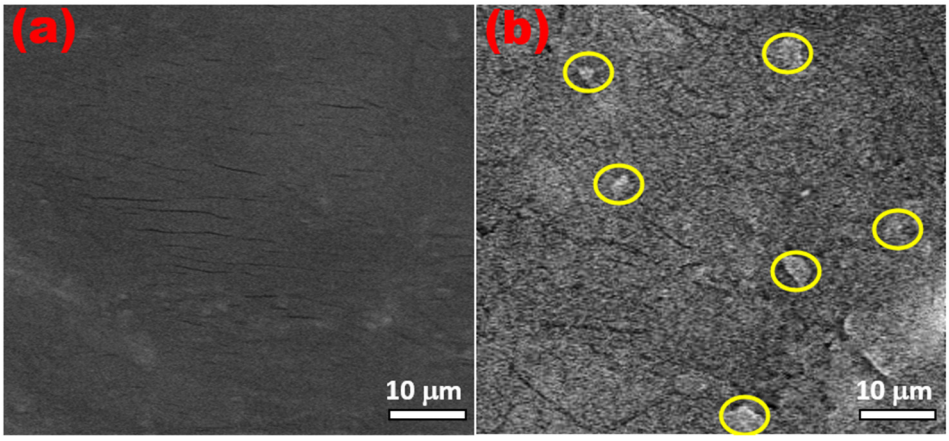

Figure 4. FESEM images of PP/$Ni_{0.9}Zn_{0.1}Fe_2O_4$ nanocomposite films containing (**a**) 0 wt% and (**b**) 15 wt%.

3.5. Thermogravimetric Analysis

Figure 5 presents TGA/DTG plots of PP/$Ni_{0.9}Zn_{0.1}Fe_2O_4$ nanocomposite films. It is clear that each curve exhibits a single degradation stage with a peak temperature within the range of 467–499 °C. The peak temperature is slightly affected by the addition of $Ni_{0.9}Zn_{0.1}Fe_2O_4$ NPs to the PP matrix. As the $Ni_{0.9}Zn_{0.1}Fe_2O_4$ NPs concentration increases, the mass losses of PP/$Ni_{0.9}Zn_{0.1}Fe_2O_4$ nanocomposite films decrease, which is consistent with previous research [63,71]. As the nanoparticle loading increases (10 wt% and 15 wt%), the interfacial interaction between the nanoparticles and the polypropylene matrix

becomes more significant compared to low loadings (5 wt%). This interaction can act as a barrier to the diffusion of volatile decomposition products, hindering the degradation process and leading to an increase in peak temperature. In comparison to pure PP, the addition of nanoparticles in the polymer matrix improved the thermal characteristics of polymer nanocomposite, as listed in Table 2. The high crosslinking density and secondary connections conferred upon $Ni_{0.9}Zn_{0.1}Fe_2O_4$ NPs with the polymer chains can be attributed to the enhancement of the thermal stability of the nanocomposites. Also, the incorporation of nanoparticles into the polymer matrix restricted polymer chain movement, reduced free radical exchange and hence decreased heat degradation [63,72].

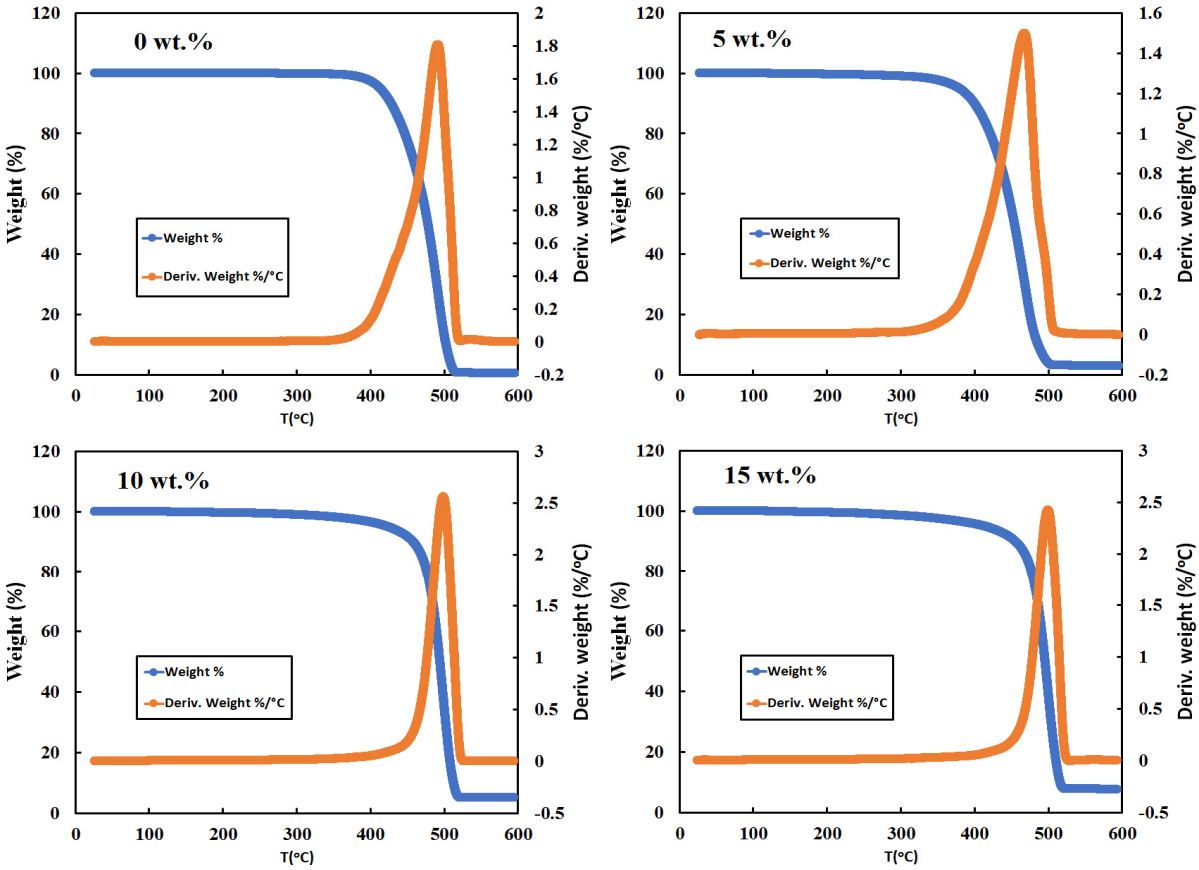

Figure 5. TGA/DTG plots of PP/$Ni_{0.9}Zn_{0.1}Fe_2O_4$ nanocomposites.

Table 2. TGA data of polypropylene loaded with $Ni_{0.9}Zn_{0.1}Fe_2O_4$.

$Ni_{0.9}Zn_{0.1}Fe_2O_4$ NPs Percentage (wt%)	Degradation Stage			Mass Loss (%)			
	ΔT (°C)	T_{peak} (°C)	Mass Loss (%)	Δ m_{250}	Δ m_{350}	Δ m_{450}	Δ m_{550}
0	353–594	490	99.64	0.17	0.44	22.05	99.58
5	311–594	467	97.00	0.66	2.36	44.27	97.04
10	342–596	498	94.89	0.69	1.94	8.3	94.83
15	322–596	499	92.38	0.96	2.65	9.07	92.27

The degree of conversion (α) can be used to express the reaction rate using the following Equation (1) [73]:

$$\alpha = \frac{m_i - m_t}{m_i - m_f} \quad (1)$$

where m_i, m_f, and m_t are the initial, final, and current sample mass at the instant t.

The Coats–Redfern approximation method is a powerful tool for analyzing thermogravimetric analysis (TGA) data, particularly in the context of studying thermal decomposition processes [6,74–79]. Therefore, we use this method to determine the kinetics parameters of the TGA thermal decomposition stage shown in Figure 5.

$$Ln\left[-\frac{Ln(1-\alpha)}{T^2}\right] = -\frac{E_a}{RT} + Ln[\frac{AR}{\varphi E_a}] \quad (2)$$

where E_a, R, A, and φ are the activation energy, the real gas constant, the reaction rate constant, and the heating rate, respectively. Equation (2) states that straight-line results from plotting $Ln\left[-\frac{Ln(1-\alpha)}{T^2}\right]$ versus $\frac{1000}{T}$ with a slope and intercept directly proportional to the E_a and A, respectively as depicted in Figure 6. Estimated activation energies of the nanocomposites are reduced as $Ni_{0.9}Zn_{0.1}Fe_2O_4$ NPs are added, indicating that $Ni_{0.9}Zn_{0.1}Fe_2O_4$ NPs have a significant impact on the PP. Additionally, the following well-known formulae [78,80,81] were used to compute the changes in entropy (ΔS*), enthalpy (ΔH*), and Gibbs free energy (ΔG*) of the activation:

$$\Delta S^* = R\left[Ln\left(\frac{Ah}{K_B T_p}\right) - 1\right] \quad (3)$$

$$\Delta H^* = E_a - RT_p \quad (4)$$

$$\Delta G^* = \Delta H^* - \Delta S^* T_p \quad (5)$$

where T_p is the peak temperature of the DTG curve, k_B is the Boltzmann constant, and h is the Plank constant. Entropy (ΔS^*) and enthalpy (ΔH^*) provide information on the system's level of order, total thermal motion, and Gibbs or free energy (ΔG^*) provides information on the stability of the system.

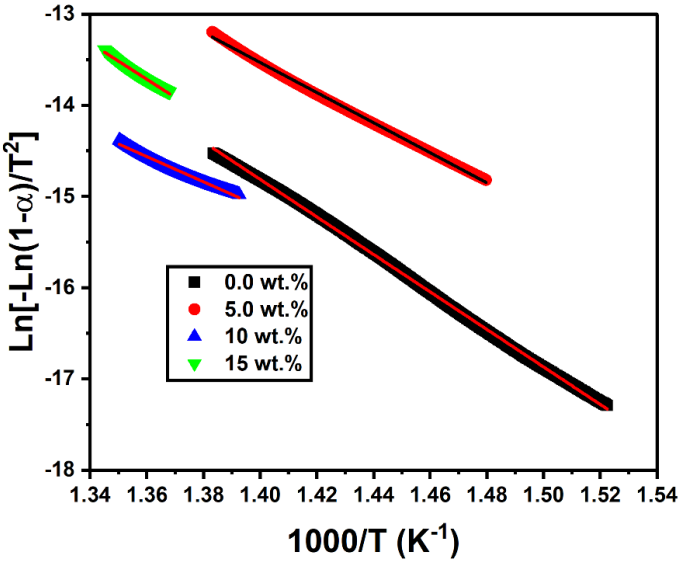

Figure 6. Coats–Redfern estimations for PP/$Ni_{0.9}Zn_{0.1}Fe_2O_4$ nanocomposites.

The values of the computed thermodynamic parameters (E_a, ΔS^*, ΔH^*, and ΔG^*) are listed in Table 3 in accordance with the Coats–Redfern method. It is evident that as the $Ni_{0.9}Zn_{0.1}Fe_2O_4$ NP concentrations rise, the values of all thermodynamic parameters fall. This can be explained by noting that when NPs rise, random macromolecule chain scission prevails in polymeric matrices, and activation energy decreases. Additionally, each sample has negative entropy, indicating ordered systems and potentially more ordered activated

states that could result from the chemisorption of other light sources. The values of E_a, ΔS^*, ΔH^*, and ΔG^* in our work are less than in [74].

Table 3. Thermal kinetic parameters for PP/$Ni_{0.9}Zn_{0.1}Fe_2O_4$ nanocomposites.

$Ni_{0.9}Zn_{0.1}Fe_2O_4$ NPs Percentage (wt%)	E_a (KJ/mol)	A (S^{-1})	ΔS* (J/mol.K)	ΔH* (KJ/mol)	ΔG* (KJ/mol)
0	393.83	2.64×10^{11}	−38.70	389.75	408.71
5	315.83	2.55×10^{9}	−76.90	311.95	347.89
10	264.67	1.04×10^{7}	−123.18	260.53	321.90
15	381.55	1.41×10^{11}	−44.08	377.40	399.39

3.6. Dielectric Measurements

Figure 7 illustrates the frequency dependence of the real dielectric constant (ε') of PP and its nanocomposites at room temperature in the frequency range 20 Hz $\leq f \leq$ 2 MHz. Over most of the frequency range studied, the dielectric constants of the polymer nanocomposites were almost frequency-independent. Polarizations relate to the PP matrix, $Ni_{0.9}Zn_{0.1}Fe_2O_4$ NPs, and PP-NPs interfaces in this study, although the nonpolar character of PP may have a major effect on the tiny dielectric response at the applied frequency range. Some polymer nanocomposites have previously shown the same characteristic [39,82–84]. The dependence of ε' on $Ni_{0.9}Zn_{0.1}Fe_2O_4$ NPs concentration exhibited an enhancement with rising NP concentrations for weight ratios ranging from 0 to 15 wt%. This strong dependence of ε' on nanofiller concentration has already been found for nanocomposites [63,64,85–91]. The good interaction between NPs and the PP matrix is confirmed via such behavior. Basically, it can be attributed to the formation of microcapacitor networks in the PP matrix as the content of the nanofiller rises. The accumulation of charge carriers in the interior surface of the PP matrix may also be the cause of this increase, as shown by the Maxwell–Wagner–Sillars effects [64,92,93]. The 15 wt% modified film has a lower dielectric constant than other nanocomposite films, which could be because of cluster formation [6].

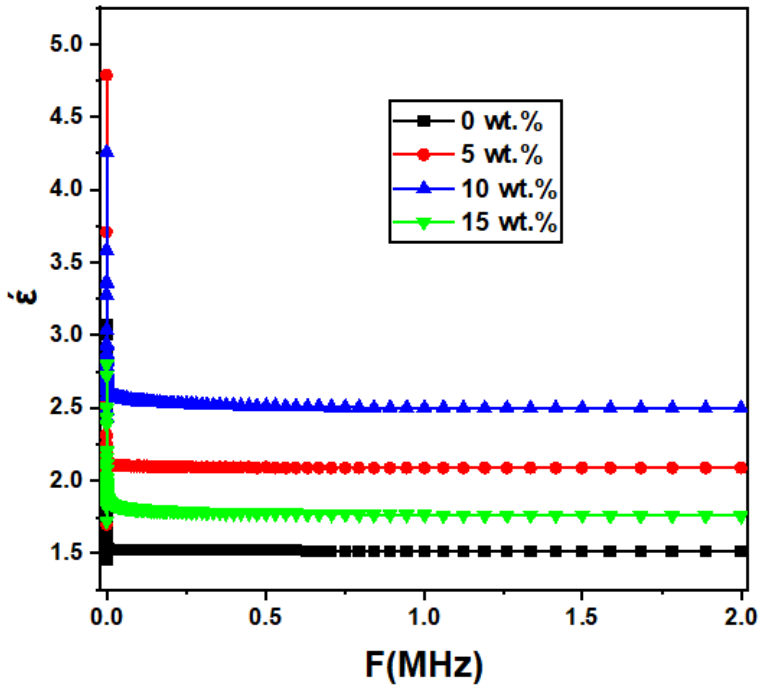

Figure 7. The plot of ε' against the frequency for PP/$Ni_{0.9}Zn_{0.1}Fe_2O_4$ nanocomposites.

Figure 8 shows the variation in dielectric loss ($\log(\varepsilon'')$) with angular frequency $\log(\omega)$ for PP/$Ni_{0.9}Zn_{0.1}Fe_2O_4$ nanocomposites films at room temperature. Generally, every specimen behaves in the same way as depicted, decreasing as frequency rises and then increasing at higher frequencies. The minimum dielectric loss shifts to higher frequencies as $Ni_{0.9}Zn_{0.1}Fe_2O_4$ Nps content increases. Equation (6) [94] gives the frequency-dependence relationship of ε'':

$$\varepsilon''(\omega) = (\varepsilon_s - \varepsilon_\infty)2\pi^2 N\left(\frac{ne^2}{\varepsilon_s}\right)^3 K_B T \tau_o^m W_m^{-4} \omega^m \quad (6)$$

where

$$m = -\frac{K_B T}{W_m}$$

where ε_s, ε_∞, n, N, e, k_β, T, τ_o, and W_m, are static permittivity, infinity permittivity, number of electrons, the concentration of localized sites, elementary charge, Boltzmann's constant, absolute temperature, relaxation time, the energy required to move an electron from one site to the infinite, and angular frequency. By applying this model to our results and fitting a portion of the data in the frequency range of 20 Hz to 84 kHz to a linear equation, we may find the values of W_m presented in Table 3. Generally, the values of W_m tabulated in Table 3 are greater than those of PVC/NiO (0.025–0.027 eV) [92] but lower than those of Polyester/$Ni_{0.5}Zn_{0.5}Fe_2O_4$ (0.16–0.43 eV) [64], and their values grew as the $Ni_{0.9}Zn_{0.1}Fe_2O_4$ Nps concentration increased.

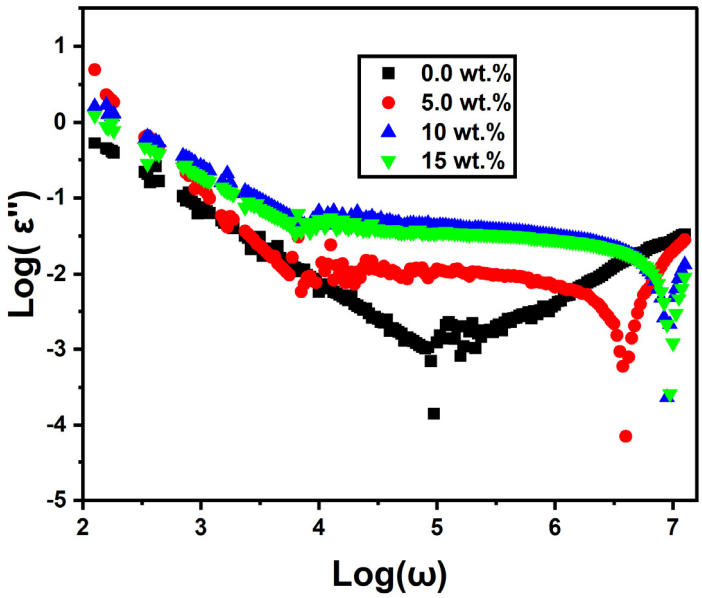

Figure 8. The variation in dielectric loss versus Log(ω) for PP/$Ni_{0.9}Zn_{0.1}Fe_2O_4$ nanocomposite films.

The variation in the tangent loss (tan(δ)) of PP loaded with different weight ratios of $Ni_{0.9}Zn_{0.1}Fe_2O_4$ NPs at room temperature in the frequency range 20 Hz to 2 MHz is displayed in Figure 9. The measured values of tan(δ) of PP nanocomposites are frequency-dependent at all frequency ranges, as can be seen. For PP, the tangent loss initially has high values at low frequencies and rapidly decreases as the frequency rises to 4226 Hz; thereafter, the tangent loss increases. Tan(δ) for the PP is consistent with the strong conductivity at high frequencies associated with charge carrier hopping or tunneling [63,64]. The trendlines of the nanocomposites feature two regions: the first region shows a decrease in tan (δ) with frequency due to a reduction in dielectric dispersion or because the nanocomposite films' crystallinity has improved [95], while the second region exhibits an increase in loss tangent

with frequency. The nanocomposite films' minimal loss tangents are, respectively, at 0.6325, 1.416, and 1.5 MHz and 5, 10 and 15 wt%.

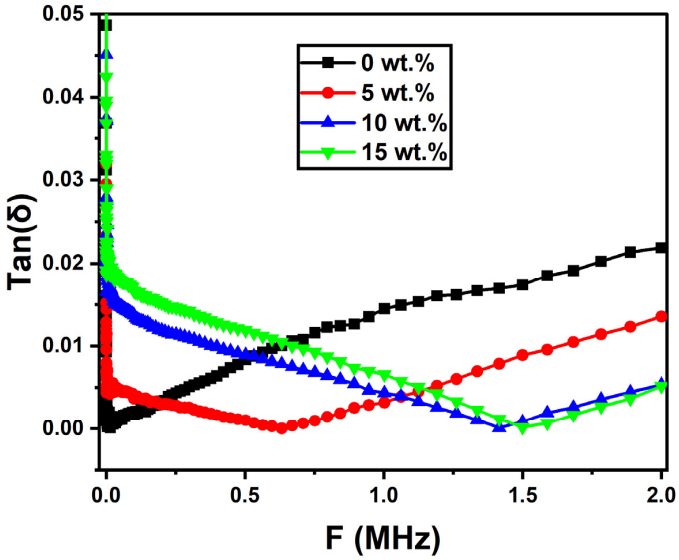

Figure 9. The frequency dependence of tan(δ) of PP/$Ni_{0.9}Zn_{0.1}Fe_2O_4$ nanocomposites films.

The Cole–Cole curves of PP/$Ni_{0.9}Z_{0.1}Fe_2O_4$ nanocomposite films at room temperature are revealed in Figure 10. The semicircle on each Cole–Cole graph represented relaxation processes. As a result, the values of static permittivity (ε_s), infinity permittivity (ε_∞), and dielectric intensity ($\Delta\varepsilon$) that are given in Table 3 are obtained by fitting these semicircles. According to Table 3, the values of ε_∞ and ε_s for films made of PP/$Ni_{0.9}Z_{0.1}Fe_2O_4$ nanocomposites are greater than those of PP, confirming that the addition of NPs increased the dielectric constant of PP.

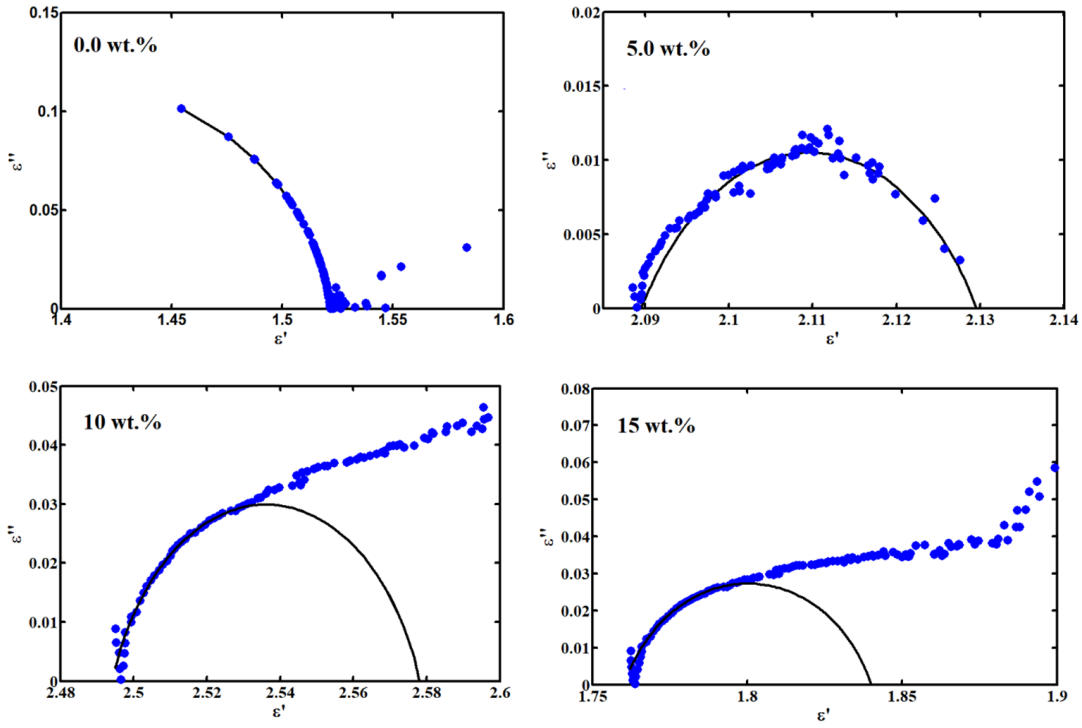

Figure 10. Cole–Cole plots of PP/$Ni_{0.9}Zn_{0.1}Fe_2O_4$ nanocomposite films.

According to the relation [96], the relaxation time (τ_o) can be estimated from the Cole–Cole analysis:

$$\ln(\frac{v}{u}) = (1-\alpha)[\ln(\omega) + \ln(\tau_o)] \quad (7)$$

where u is the distance between the experimental point and ε_∞, and v is the distance between ε_s and the experimental point on the Cole–Cole plot. According to Figure 11, the relationship between Ln(ω) and Ln(v/u) is fitted with a linear line. By knowing the slope and intercept of the fitting line, τ_o can be calculated, and by applying this equation, $\tau_o = 1/2\pi f_o$, we may determine f_o which they listed in Table 3. The obtained values of τ_o are higher than those obtained in PVC/CuO [97] and lower than Polyester/$Ni_{0.5}Zn_{0.5}Fe_2O_4$ [61]. As listed in Table 4, the relaxation time (τ_o) decreases as the $Ni_{0.9}Zn_{0.1}Fe_2O_4$ NP content increases; this behavior is shown in other works [97,98].

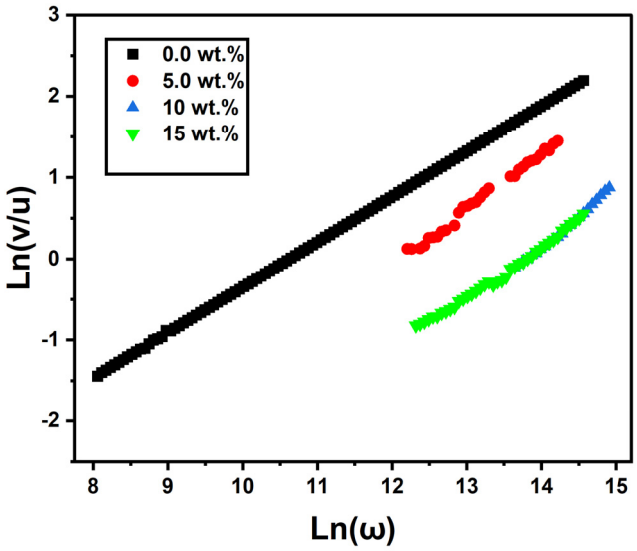

Figure 11. The relationship between ln(ω) and ln(v/u) for PP/$Ni_{0.9}Zn_{0.1}Fe_2O_4$ nanocomposites.

Table 4. The deduced ε_s, ε_∞, $\Delta\varepsilon$, τ_o, f_o, and W_m of PP/$Ni_{0.9}Zn_{0.1}Fe_2O_4$ nanocomposites.

$Ni_{0.9}Zn_{0.1}Fe_2O_4$ NPs Percentage (wt.%)	ε_s	ε_∞	$\Delta\varepsilon$	τ_o (μs)	f_o (kHz)	W_m (eV)
0	1.52	1.26	0.26	24.2	6.58	0.106
5	2.13	2.09	0.04	5.42	29.36	0.068
10	2.58	2.49	0.09	0.99	160.76	0.119
15	1.84	1.76	0.08	1.05	151.58	0.126

Figure 12 depicts the variation in the AC impedance (Z′) of the PP/$Ni_{0.9}Zn_{0.1}Fe_2O_4$ nanocomposite within the frequency range of 20 Hz $\leq f \leq$ 2 MHz at room temperature. The values of Z′ fall with frequency and attain nearly minimal constant values at high frequencies, which can be explained in part by charge carrier hopping or tunneling. The polymer nanocomposite films' improved crystallinity, which results in less hopping interchain and intrachain ion movements, caused the inclusion of nanoparticles to also provide an improvement in Z′ values [99].

$Ni_{0.9}Z_{0.1}Fe_2O_4$ is a spinel ferrite with good electrical conductivity due to the presence of mixed valence states (Fe^{2+} and Fe^{3+}) and the hopping mechanism of charge carriers. When incorporated into the PP matrix, it creates conductive pathways, reducing the overall impedance of the composite and thereby increasing Z′. Meanwhile, the interface between the $Ni_{0.9}Z_{0.1}Fe_2O_4$ nanoparticles and the PP matrix creates an additional layer with unique

electrical properties. This interfacial region can exhibit polarization under an applied electric field, contributing to the overall impedance response and potentially increasing Z′. Moreover, the presence of $Ni_{0.9}Z_{0.1}Fe_2O_4$ nanoparticles can trap mobile ions and electrons within the PP matrix, preventing them from accumulating at the electrode interfaces. This reduces space charge buildup, which can contribute to leakage current and lower Z′ values [100].

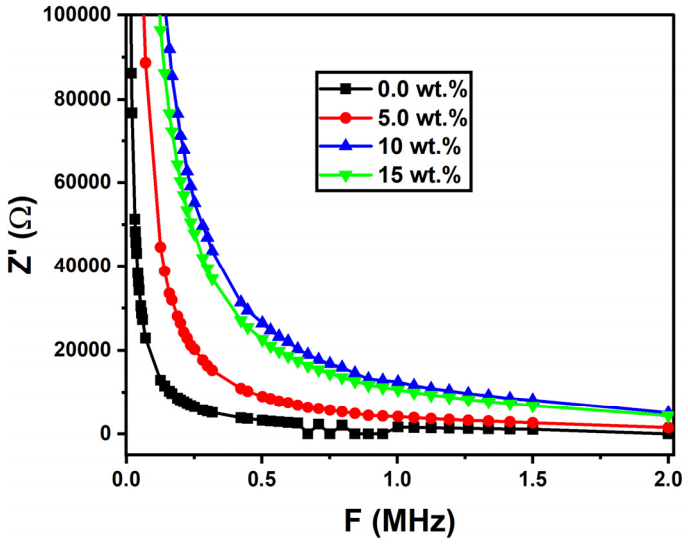

Figure 12. The plot of the real part of AC impedance versus frequency of PP/$Ni_{0.9}Z_{0.1}Fe_2O_4$ nanocomposites.

4. Conclusions

The successful synthesis of PP/$Ni_{0.9}Zn_{0.1}Fe_2O_4$ nanocomposites was achieved and confirmed via structural techniques involving XRD, FTIR, and SEM. Further, TEM, XRD, and TEM findings revealed an average crystal size of approximately 29 nm for the $Ni_{0.9}Zn_{0.1}Fe_2O_4$ nanoparticles. TEM images also confirmed the spherical morphology and lack of aggregation of the nanoparticles. FESEM micrographs demonstrated the successful incorporation of the $Ni_{0.9}Zn_{0.1}Fe_2O_4$ NPs into the polymer matrix. TGA/DTG analysis showed improved thermal characteristics and reduced weight loss. However, the peak temperature range shifted between 468 and 499 °C upon introducing $Ni_{0.9}Zn_{0.1}Fe_2O_4$ NPs. Kinetic and thermodynamic parameters, including activation energy, enthalpy, entropy, and Gibbs free energy, were determined from TGA/DTG data using the Coats–Redfern equation. Notably, the values of Ea, ΔS, ΔH, and ΔG* decreased with increasing $Ni_{0.9}Zn_{0.1}Fe_2O_4$ content. Dielectric loss and AC impedance exhibited dependence on both frequency and composition. The real part of the complex permittivity (e′) increased with the addition of $Ni_{0.9}Zn_{0.1}Fe_2O_4$ NPs. Cole–Cole analysis revealed a single relaxation semicircle and provided values for ε_s, ε_∞, $\Delta\varepsilon$, τ_0, and f_o. The combination of dielectric and magnetic properties of PP/$Ni_{0.9}Zn_{0.1}Fe_2O_4$ nanocomposites suggests potential use in electromagnetic interference (EMI) shielding materials.

Author Contributions: Conceptualization, T.A.M.T., M.T. and A.I.; methodology, T.A.M.T. and M.T.; formal analysis, T.A.M.T. and M.T.; investigation, T.A.M.T. and M.T.; resources, T.A.M.T., M.T. and A.I.; data curation, T.A.M.T., M.T. and A.I.; writing—original draft preparation, T.A.M.T., M.T. and A.I.; writing—review and editing, T.A.M.T., M.T. and A.I.; visualization, T.A.M.T., M.T. and A.I.; supervision, T.A.M.T., M.T. and A.I.; project administration, T.A.M.T., M.T. and A.I.; funding acquisition, T.A.M.T., M.T. and A.I. All authors have read and agreed to the published version of the manuscript.

Funding: This research received no external funding.

Data Availability Statement: Data will be made available upon reasonable request.

Conflicts of Interest: The authors declare that they have no known competing financial interests or personal relationships that could have appeared to influence the work reported in this paper.

References

1. Badawi, A. Characterization of the optical and mechanical properties of CdSe QDs/PMMA nanocomposite films. *J. Mater. Sci. Mater. Electron.* **2015**, *26*, 3450–3457. [CrossRef]
2. Al-Osaimi, J.; Al-Hosiny, N.; Abdallah, S.; Badawi, A. Characterization of optical, thermal and electrical properties of SWCNTs/PMMA nanocomposite films. *Iran. Polym. J.* **2014**, *23*, 437–443. [CrossRef]
3. Guo, M.; Jiang, J.; Shen, Z.; Lin, Y.; Nan, C.W.; Shen, Y. High-energy-density ferroelectric polymer nanocomposites for capacitive energy storage: Enhanced breakdown strength and improved discharge efficiency. *Mater. Today* **2019**, *29*, 49–67. [CrossRef]
4. Donya, H.; Taha, T.A.; Alruwaili, A.; Tomsah, I.B.I.; Ibrahim, M. Micro structure and optical spectroscopy of PVA/iron oxide polymer nanocomposites. *J. Mater. Res. Technol.* **2020**, *9*, 9189–9194. [CrossRef]
5. Taha, T.A.M.; Alanazi SSSEl-Nasser, K.; Alshammari, A.H.; Ismael, A. Structure–Property Relationships in PVDF/$SrTiO_3$/CNT Nanocomposites for Optoelectronic and Solar Cell Applications. *Polymers* **2024**, *16*, 736. [CrossRef]
6. Taha, T.A.; Mahmoud, M.H.; Hamdeh, H.H. Development, thermal and dielectric investigations of PVDF-Y_2O_3 polymer nanocomposite films. *J. Polym. Res.* **2021**, *28*, 148. [CrossRef]
7. Taha, T.A.; Alzara, M.A.A. Synthesis, thermal and dielectric performance of PVA-$SrTiO_3$ polymer nanocomposites. *J. Mol. Struct.* **2021**, *1238*, 130401. [CrossRef]
8. Alhassan, S.; Alshammari, K.; Alshammari, M.; Alotaibi, T.; Alshammari, A.H.; Alhamazani, A.; Taha, T.A.M. Linear and nonlinear optical investigations of polyvinyl chloride modified La_2O_3 nanocomposite films. *Results Phys.* **2024**, *58*, 107456. [CrossRef]
9. Alshammari, A.H.; Alhassan, S.; Iraqi, A.; Saad, S.A.; Taha, T.A.M. Dielectric relaxation investigations of polyester/$CoFe_2O_4$ composites. *J. Mater. Sci. Mater. Electron.* **2023**, *34*, 2132. [CrossRef]
10. Kim, W.S.; Song, H.S.; Lee, B.O.; Kwon, K.H.; Lim, Y.S.; Kim, M.S. Electrical properties of PVDF/PVP composite filled with carbon nanotubes prepared by floating catalyst method. *Macromol. Res.* **2002**, *10*, 253–258. [CrossRef]
11. Barber, P.; Balasubramanian, S.; Anguchamy, Y.; Gong, S.; Wibowo, A.; Gao, H.; Ploehn, H.J.; Zur Loye, H.C. Polymer composite and nanocomposite dielectric materials for pulse power energy storage. *Materials* **2009**, *2*, 1697–1733. [CrossRef]
12. Li, D.G.; Chen, C.; Rao, W.; Lu, W.H.; Xiong, Y.H. Preparation and microwave absorption properties of polyaniline/$Mn_{0.8}Zn_{0.2}Fe_2O_4$ nanocomposite in 2–18 GHz. *J. Mater. Sci. Mater. Electron.* **2014**, *25*, 76–81. [CrossRef]
13. Fang, X.; Ma, J.; Gu, C.; Xiong, W.; Jiang, T. Synchronous enhancement of electromagnetic and chemical effects-induced quantitative adsorptive detection of quercetin based on flexible polymer-silver-ZIF-67 SERS substrate. *Sens. Actuators B Chem.* **2023**, *378*, 133176. [CrossRef]
14. Song, F.; Shen, X.; Liu, M.; Xiang, J. Preparation and magnetic properties of $SrFe_{12}O_{19}$/$Ni_{0.5}Zn_{0.5}Fe_2O_4$ nanocomposite ferrite microfibers via sol–gel process. *Mater. Chem. Phys.* **2011**, *126*, 791–796. [CrossRef]
15. Mohamed, M.B.; Abdel-Kader, M.H. Effect of excess oxygen content within different nano-oxide additives on the structural and optical properties of PVA/PEG blend. *Appl. Phys. A* **2019**, *125*, 209. [CrossRef]
16. Nangia, R.; Shukla, N.K.; Sharma, A. Optical and structural properties of $Se_{80}Te_{15}Bi_5$/PVA nanocomposite films. *J. Mol. Struct.* **2019**, *1177*, 323–330. [CrossRef]
17. Soliman, T.S.; Vshivkov, S.A. Effect of Fe nanoparticles on the structure and optical properties of polyvinyl alcohol nanocomposite films. *J. Non-Cryst. Solids* **2019**, *519*, 119452. [CrossRef]
18. Choudhary, S.; Sengwa, R.J. Investigation on structural and dielectric properties of silica nanoparticles incorporated poly (ethylene oxide)/poly (vinyl pyrrolidone) blend matrix based nanocomposites. *J. Inorg. Organomet. Polym. Mater.* **2019**, *29*, 592–607. [CrossRef]
19. Su, J.; Zhang, J. Recent development on modification of synthesized barium titanate ($BaTiO_3$) and polymer/$BaTiO_3$ dielectric composites. *J. Mater. Sci. Mater. Electron.* **2019**, *30*, 1957–1975. [CrossRef]
20. Aziz, S.B.; Hassan, A.Q.; Mohammed, S.J.; Karim, W.O.; Kadir, M.F.Z.; Tajuddin, H.A.; Chan, N.N.M.Y. Structural and optical characteristics of PVA: C-Dot composites: Tuning the absorption of ultraviolet (UV) region. *Nanomaterials* **2019**, *9*, 216. [CrossRef]
21. Nawar, A.M.; Mohammed, M.I.; Yahia, I.S. Facile synthesis and optical characterization of graphene oxide-doped TiO_2/polyvinyl alcohol nanocomposites: Optical limiting applications. *Mater. Res. Express* **2019**, *6*, 075054. [CrossRef]
22. Stepanov, A.L. Optical properties of polymer nanocomposites with functionalized nanoparticles. In *Polymer Composites with Functionalized Nanoparticles*; Elsevier: Amsterdam, The Netherlands, 2019; pp. 325–355.
23. Banerjee, M.; Jain, A.; Mukherjee, G.S. Microstructural and optical properties of polyvinyl alcohol/manganese chloride composite film. *Polym. Compos.* **2019**, *40*, E765–E775. [CrossRef]
24. Aziz, S.B. Modifying poly(vinyl alcohol) (PVA) from insulator to small-bandgap polymer: A novel approach for organic solar cells and optoelectronic devices. *J. Electron. Mater.* **2016**, *45*, 736–745. [CrossRef]
25. Fu, Y.; Chen, H.; Sun, X.; Wang, X. Combination of cobalt ferrite and graphene: High-performance and recyclable visible-light photocatalysis. *Appl. Catal. B Environ.* **2012**, *111*, 280–287. [CrossRef]
26. Sankaranarayanan, V.K.; Pankhurst, Q.A.; Dickson, D.P.E.; Johnson, C.E. An investigation of particle size effects in ultrafine barium ferrite. *J. Magn. Magn. Mater.* **1993**, *125*, 199–208. [CrossRef]

27. Sankaranarayanan, V.K.; Gajbhiye, N.S. Low-Temperature Preparation of Ultrafine Rare-Earth Iron Garnets. *J. Am. Ceram. Soc.* **1990**, *73*, 1301–3007. [CrossRef]
28. Virden, A.E.; O'Grady, K. Structure and magnetic properties of NiZn ferrite nanoparticles. *J. Magn. Magn. Mater.* **2005**, *290*, 868–870. [CrossRef]
29. Kim, K.H.; Kim, Y.A.; Yamaguchi, M. Radio frequency characteristics of Fe-filled carbon nanotube film. *J. Magn. Magn. Mater.* **2006**, *302*, 232–236. [CrossRef]
30. Kubade, P.; Tambe, P. Influence of halloysite nanotubes (HNTs) on morphology, crystallization, mechanical and thermal behaviour of PP/ABS blends and its composites in presence and absence of dual compatibilizer. *Compos. Interfaces* **2016**, *23*, 433–451. [CrossRef]
31. Kubade, P.; Tambe, P. Influence of surface modification of halloysite nanotubes and its localization in PP phase on mechanical and thermal properties of PP/ABS blends. *Compos. Interfaces* **2017**, *24*, 469–487. [CrossRef]
32. Tambe, P.; Sharma, A.; Kulkarni, H.; Panda, B. Influence of surface treated halloysite nanotubes on mechanical and thermal properties of polypropylene nanocomposites. *Mater. Today Proc.* **2022**, *56*, 1351–1355. [CrossRef]
33. Lohar, G.; Tambe, P.; Jogi, B. Influence of dual compatibilizer and carbon black on mechanical and thermal properties of PP/ABS blends and their composites. *Compos. Interfaces* **2020**, *27*, 1101–1136. [CrossRef]
34. Jogi, B.F.; Lohar, G.; Pankaj, T. Influence of carbon black (CB) on 80/20 (wt/wt) poly-propylene (PP)/acrylonitrile-butadiene-styrene (ABS) nanocomposites: Localization, morphological behavior, crystallinity and thermal stability. In *AIP Conference Proceedings*; AIP Publishing LLC: Melville, NY, USA, 2021; Volume 2341, p. 040014.
35. Patil, J.; Patil, H.; Sankpal, R.; Rathod, D.; Patil, K.; Kubade, P.R.; Kulkarni, H.B. Studies on mechanical and thermal performance of carbon nanotubes/polypropylene nanocomposites. *Mater. Today Proc.* **2021**, *46*, 7182–7186. [CrossRef]
36. Krishnaiah, P.; Manickam, S.; Ratnam, C.T.; Raghu, M.S.; Parashuram, L.; Prashantha, K.; Jeon, B.H. Surface-treated short sisal fibers and halloysite nanotubes for synergistically enhanced performance of polypropylene hybrid composites. *J. Thermoplast. Compos. Mater.* **2020**, *35*, 2089–2104. [CrossRef]
37. Liu, W.; Cheng, L.; Li, S. Review of electrical properties for polypropylene based nanocomposite. *Compos. Commun.* **2018**, *10*, 221–225. [CrossRef]
38. Furlan, L.G.; Ferreira, C.I.; Dal Castel, C.; Santos, K.S.; Mello, A.C.E.; Liberman, S.A.; Oviedo, M.A.S.; Mauler, R.S. Effect of processing conditions on the mechanical and thermal properties of high-impact polypropylene nanocomposites. *Mater. Sci. Eng. A* **2011**, *528*, 6715–6718. [CrossRef]
39. Uyor, U.O.; Popoola, A.P.I.; Popoola, O.M.; Aigbodion, V.S. Thermal, mechanical and dielectric properties of functionalized sandwich BN-$BaTiO_3$-BN/polypropylene nanocomposites. *J. Alloys Compd.* **2022**, *894*, 162405. [CrossRef]
40. Siddiqui, M.T.H.; Baloch, H.A.; Nizamuddin, S.; Kashi, S.; Tanjung, F.A.; Hossain, N.; Mazari, S.A.; Mubarak, N.M.; Griffin, G.J.; Srinivasan, M. Thermal, mechanical, rheological, electrical and electromagnetic interference shielding performance of polypropylene/magnetic carbon nanocomposites. *J. Environ. Chem. Eng.* **2021**, *9*, 105447. [CrossRef]
41. Sonawane, S.; Thakur, P.; Paul, R. Study on thermal property enhancement of MWCNT based polypropylene (PP) nanocomposites. *Mater. Today Proc.* **2020**, *27*, 550–555. [CrossRef]
42. Rishaban, R.; Balakrishnan, G.; Hema, R. Synthesis and properties of polypropylene-graphene nanocomposite. *Mater. Today Proc.* **2022**, *62*, 1977–1983. [CrossRef]
43. Bendaoued, A.; Messaoud, M.; Harzallah, O.; Bistac, S.; Salhi, R. Nano-TiO_2 effect on thermal, rheological and structural properties of thermoplastic polypropylene nanocomposites. *J. Mater. Res. Technol.* **2022**, *17*, 2313–2325. [CrossRef]
44. Mandal, D.K.; Bhunia, H.; Bajpai, P.K.; Chaudhari, C.V.; Dubey, K.A.; Varshney, L.; Kumar, A. Preparation and characterization of polypropylene/polylactide blends and nanocomposites and their biodegradation study. *J. Thermoplast. Compos. Mater.* **2021**, *34*, 725–744. [CrossRef]
45. Tambe, P.B.; Bhattacharyya, A.R.; Kamath, S.S.; Kulkarni, A.R.; Sreekumar, T.V.; Srivastav, A.; Rao, K.B.; Liu, Y.; Kumar, S. Structure–property relationship studies in amine functionalized multiwall carbon nanotubes filled polypropylene composite fiber. *Polym. Eng. Sci.* **2012**, *52*, 1183–1194. [CrossRef]
46. Tambe, P.B.; Bhattacharyya, A.R.; Kulkarni, A.R. The influence of melt-mixing process conditions on electrical conductivity of polypropylene/multiwall carbon nanotubes composites. *J. Appl. Polym. Sci.* **2013**, *127*, 1017–1026. [CrossRef]
47. Lohar, G.; Tambe, P.; Jogi, B. Migration induced localization of multiwalled carbon nanotubes in PP phase of PP/ABS blend and their hybrid composites: Influence on mechanical and thermal properties. *Mater. Today Proc.* **2022**, *49*, 1215–1224. [CrossRef]
48. Yeole, P.; Alwekar, S.; Veluswamy, N.K.P.; Kore, S.; Hiremath, N.; Vaidya, U.; Theodore, M. Characterization of textile-grade carbon fiber polypropylene composites. *Polym. Polym. Compos.* **2021**, *29*, 652–659. [CrossRef]
49. Alzebdeh, K.I.; Nassar, M.M.; Arunachalam, R. Effect of fabrication parameters on strength of natural fiber polypropylene composites: Statistical assessment. *Measurement* **2019**, *146*, 195–207. [CrossRef]
50. Pak, S.; Park, S.; Song, Y.S.; Lee, D. Micromechanical and dynamic mechanical analyses for characterizing improved interfacial strength of maleic anhydride compatibilized basalt fiber/polypropylene composites. *Compos. Struct.* **2018**, *193*, 73–79. [CrossRef]
51. Wang, D.; Xuan, L.; Han, G.; Wong, A.H.; Wang, Q.; Cheng, W. Preparation and characterization of foamed wheat straw fiber/polypropylene composites based on modified nano-TiO_2 particles. *Compos. Part A Appl. Sci. Manuf.* **2020**, *128*, 105674. [CrossRef]

52. Awad, S.A.; Khalaf, E.M. Investigation of improvement of properties of polypropylene modified by nano silica composites. *Compos. Commun.* **2019**, *12*, 59–63. [CrossRef]
53. Liang, J.Z. Effects of tension rates and filler size on tensile properties of polypropylene/graphene nano-platelets composites. *Compos. Part B Eng.* **2019**, *167*, 241–249. [CrossRef]
54. Klapiszewski, Ł.; Grząbka-Zasadzińska, A.; Borysiak, S.; Jesionowski, T. Preparation and characterization of polypropylene composites reinforced by functional ZnO/lignin hybrid materials. *Polym. Test.* **2019**, *79*, 106058. [CrossRef]
55. Sivakumar, N.; Narayanasamy, A.; Ponpandian, N.; Greneche, J.M.; Shinoda, K.; Jeyadevan, B.; Tohji, K. Effect of mechanical milling on the electrical and magnetic properties of nanostructured $Ni_{0.5}Zn_{0.5}Fe_2O_4$. *J. Phys. D Appl. Phys.* **2006**, *39*, 4688. [CrossRef]
56. Astafyev, A.; Lysenko, E.; Surzhikov, A.; Nikolaev, E.; Vlasov, V. Thermomagnetometric analysis of nickel–zinc ferrites. *J. Therm. Anal. Calorim.* **2020**, *142*, 1775–1781. [CrossRef]
57. Kumbhar, S.S.; Mahadik, M.A.; Mohite, V.S.; Rajpure, K.Y.; Kim, J.H.; Moholkar, A.V.; Bhosale, C.H. Structural, dielectric and magnetic properties of Ni substituted zinc ferrite. *J. Magn. Magn. Mater.* **2014**, *363*, 114–120. [CrossRef]
58. Taha, T.A.; Elrabaie, S.; Attia, M.T. Green synthesis, structural, magnetic, and dielectric characterization of $NiZnFe_2O_4$/C nanocomposite. *J. Mater. Sci. Mater. Electron.* **2018**, *29*, 18493–18501. [CrossRef]
59. Machado, G.; Denardin, E.L.G.; Kinast, E.J.; Gonçalves, M.C.; De Luca, M.A.; Teixeira, S.R.; Samios, D. Crystalline properties and morphological changes in plastically deformed isotatic polypropylene evaluated by X-ray diffraction and transmission electron microscopy. *Eur. Polym. J.* **2005**, *41*, 129–138. [CrossRef]
60. Ummartyotin, S.; Pechyen, C. Microcrystalline-cellulose and polypropylene based composite: A simple, selective and effective material for microwavable packaging. *Carbohydr. Polym.* **2016**, *142*, 133–140. [CrossRef] [PubMed]
61. Akinci, A.; Akbulut, H.; Yilmaz, F. The effect of the red mud on polymer crystallization and the interaction between the polymer-filler. *Polym.-Plast. Technol. Eng.* **2007**, *46*, 31–36. [CrossRef]
62. Mahrous, N.; Motawie, A.M.; Hakim, A.E.A.; Eid, A.I.; El-Sawey, A.A.A.-M. Study of some polypropylene nanocomposite properties. *Egypt. J. Chem.* **2018**, *61*, 825–842. [CrossRef]
63. Taha, T.A.; Elrabaie, S.; Attia, M.T. Exploring the structural, thermal and dielectric properties of PVA/$Ni_{0.5}Zn_{0.5}Fe_2O_4$ composites. *J. Electron. Mater.* **2019**, *48*, 6797–6806. [CrossRef]
64. Taha, T.A.; Hassona, A.; Elrabaie, S.; Attia, M.T. Micro-structure, thermal, and dielectric performance of polyester nanocomposites containing nano-$Ni_{0.5}Zn_{0.5}Fe_2O_4$. *Appl. Phys. A* **2020**, *126*, 761. [CrossRef]
65. Saito, T.; Okamoto, M. Polypropylene-based nano-composite formation: Delamination of organically modified layered filler via solid-state processing. *Polymer* **2010**, *51*, 4238–4242. [CrossRef]
66. Bhuiyan, M.K.H.; Rahman, M.M.; Mina, M.F.; Islam, M.R.; Gafur, M.A.; Begum, A. Crystalline morphology and properties of multi-walled carbon nanotube filled isotactic polypropylene nanocomposites: Influence of filler size and loading. *Compos. Part A Appl. Sci. Manuf.* **2013**, *52*, 70–79. [CrossRef]
67. Fang, J.; Zhang, L.; Sutton, D.; Wang, X.; Lin, T. Needleless melt-electrospinning of polypropylene nanofibres. *J. Nanomater.* **2012**, *2012*, 382639. [CrossRef]
68. Hedrick, S.A.; Chuang, S.S. Temperature programmed decomposition of polypropylene: In situ FTIR coupled with mass spectroscopy study. *Thermochim. Acta* **1998**, *315*, 159–168. [CrossRef]
69. Abdel-Hamid, H.M. Effect of electron beam irradiation on polypropylene films—Dielectric and FT-IR studies. *Solid-State Electron.* **2005**, *49*, 1163–1167. [CrossRef]
70. Manova, E.; Kunev, B.; Paneva, D.; Mitov, I.; Petrov, L.; Estournès, C.; D'Orléans, C.; Rehspringer, J.-L.; Kurmoo, M. Mechano-synthesis, characterization, and magnetic properties of nanoparticles of cobalt ferrite, $CoFe_2O_4$. *Chem. Mater.* **2004**, *16*, 5689–5696. [CrossRef]
71. Taha, T.A. Optical properties of PVC/Al_2O_3 nanocomposite films. *Polym. Bull.* **2019**, *76*, 903–918. [CrossRef]
72. Taha, T.A.; Ismail, Z.; Elhawary, M.M. Structural, optical and thermal characterization of PVC/SnO_2 nanocomposites. *Appl. Phys. A* **2018**, *124*, 307. [CrossRef]
73. Ebrahimi-Kahrizsangi, R.; Abbasi, M.H. Evaluation of reliability of Coats-Redfern method for kinetic analysis of non-isothermal TGA. *Trans. Nonferrous Met. Soc. China* **2008**, *18*, 217–221. [CrossRef]
74. Gaabour, L.H. Thermal spectroscopy and kinetic studies of PEO/PVDF loaded by carbon nanotubes. *J. Mater.* **2015**, *2015*, 824859. [CrossRef]
75. Peng, Z.; Kong, L.X. A thermal degradation mechanism of polyvinyl alcohol/silica nanocomposites. *Polym. Degrad. Stab.* **2007**, *92*, 1061–1071. [CrossRef]
76. Diefallah, E.H.M. Kinetic analysis of thermal decomposition reactions: Part VI. Thermal decomposition of manganese (II) acetate tetrahydrate. *Thermochim. Acta* **1992**, *202*, 1–16. [CrossRef]
77. Chetehouna, K.; Belayachi, N.; Rengel, B.; Hoxha, D.; Gillard, P. Investigation on the thermal degradation and kinetic parameters of innovative insulation materials using TGA-MS. *Appl. Therm. Eng.* **2015**, *81*, 177–184. [CrossRef]
78. Vlaev, L.; Nedelchev, N.; Gyurova, K.; Zagorcheva, M. A comparative study of non-isothermal kinetics of decomposition of calcium oxalate monohydrate. *J. Anal. Appl. Pyrolysis* **2008**, *81*, 253–262. [CrossRef]
79. Coats, A.W.; Redfern, J.P. Kinetic parameters from thermogravimetric data. *Nature* **1964**, *201*, 68–69. [CrossRef]

80. Grabchev, I.; Petkov, C.; Bojinov, V. Infrared spectral characterization of poly (amidoamine) dendrimers peripherally modified with 1,8-naphthalimides. *Dye. Pigment.* **2004**, *62*, 229–234. [CrossRef]
81. Flynn, J.H.; Wall, L.A. General treatment of the thermogravimetry of polymers. *J. Res. Natl. Bur. Stand. Sect. A Phys. Chem.* **1966**, *70*, 487. [CrossRef]
82. Tomer, V.; Polizos, G.; Randall, C.A.; Manias, E. Polyethylene nanocomposite dielectrics: Implications of nanofiller orientation on high field properties and energy storage. *J. Appl. Phys.* **2011**, *109*, 074113. [CrossRef]
83. Zhou, W.; Wang, C.; Ai, T.; Wu, K.; Zhao, F.; Gu, H. A novel fiber-reinforced polyethylene composite with added silicon nitride particles for enhanced thermal conductivity. *Compos. Part A Appl. Sci. Manuf.* **2009**, *40*, 830–836. [CrossRef]
84. Mansour, S.A.; Elsad, R.A.; Izzularab, M.A. Dielectric investigation of high-density polyethylene loaded by ZnO nanoparticles synthesized by sol–gel route. *J. Sol-Gel Sci. Technol.* **2016**, *80*, 333–341. [CrossRef]
85. Tanaka, T. Dielectric nanocomposites with insulating properties. *IEEE Trans. Dielectr. Electr. Insul.* **2005**, *12*, 914–928. [CrossRef]
86. Mansour, S.A.; Elsad, R.A.; Izzularab, M.A. Dielectric properties enhancement of PVC nanodielectrics based on synthesized ZnO nanoparticles. *J. Polym. Res.* **2016**, *23*, 85. [CrossRef]
87. Roy, M.; Nelson, J.K.; MacCrone, R.K.; Schadler, L.S.; Reed, C.W.; Keefe, R. Polymer nanocomposite dielectrics-the role of the interface. *IEEE Trans. Dielectr. Electr. Insul.* **2005**, *12*, 629–643. [CrossRef]
88. Couderc, H.; David, E.; Frechette, M. Study of water diffusion in PE-SiO_2 nanocomposites by dielectric spectroscopy. *Trans. Electr. Electron. Mater.* **2014**, *15*, 291–296. [CrossRef]
89. Zhang, Q.P.; Du, F.Y.; Liu, X.; Lv, J.H.; He, L.; Li, J.L.; Zhou, Y.L. Optimizing the dielectric constant of the shell layer in core–shell structures for enhanced energy density of polymer nanocomposites. *Phys. Chem. Chem. Phys.* **2023**, *25*, 18030–18037. [CrossRef] [PubMed]
90. Tuncer, E.; Sauers, I.; James, D.R.; Ellis, A.R.; Paranthaman, M.P.; Aytuğ, T.; Sathyamurthy, S.; More, K.L.; Li, J.; Goyal, A. Electrical properties of epoxy resin based nano-composites. *Nanotechnology* **2006**, *18*, 025703. [CrossRef]
91. Ciuprina, F.; Plesa, I.; Notingher, P.V.; Tudorache, T.; Panaitescu, D. Dielectric properties of nanodielectrics with inorganic fillers. In Proceedings of the 2008 Annual Report Conference on Electrical Insulation and Dielectric Phenomena, Quebec, QC, Canada, 26–29 October 2008; IEEE: New York, NY, USA, 2008; pp. 682–685.
92. Taha, T.A.; Hendawy, N.; El-Rabaie, S.; Esmat, A.; El-Mansy, M.K. Fluorescence and dielectric spectroscopy identification of polyvinyl chloride/NiO nanocomposites. *J. Mol. Struct.* **2020**, *1212*, 128162. [CrossRef]
93. Amor, I.B.; Rekik, H.; Kaddami, H.; Raihane, M.; Arous, M.; Kallel, A. Studies of dielectric relaxation in natural fiber–polymer composites. *J. Electrost.* **2009**, *67*, 717–722. [CrossRef]
94. Giuntini, J.C.; Zanchetta, J.V.; Jullien, D.; Eholie, R.; Houenou, P. Temperature dependence of dielectric losses in chalcogenide glasses. *J. Non-Cryst. Solids* **1981**, *45*, 57–62. [CrossRef]
95. Song, Y.; Shen, Y.; Liu, H.; Lin, Y.; Li, M.; Nan, C.W. Improving the dielectric constants and breakdown strength of polymer composites: Effects of the shape of the $BaTiO_3$ nanoinclusions, surface modification and polymer matrix. *J. Mater. Chem.* **2012**, *22*, 16491–16498. [CrossRef]
96. Usmanov, S.M.; Zaikov, G.E. *Numerical Methods of Solving Ill-Posed Problems of Dielectric Spectrometry*; Nova Publishers: Hauppauge, NY, USA, 2002.
97. Abouhaswa, A.S.; Taha, T.A. Tailoring the optical and dielectric properties of PVC/CuO nanocomposites. *Polym. Bull.* **2020**, *77*, 6005–6016. [CrossRef]
98. Shukla, N.; Thakur, A.K.; Shukla, A.; Chatterjee, R. Dielectric relaxation and thermal studies on dispersed phase polymer nanocomposite films. *J. Mater. Sci. Mater. Electron.* **2014**, *25*, 2759–2770. [CrossRef]
99. Sadiq, M.; Arya, A.; Ali, J.; Singh, N.P.; Sharma, A.L. Electrical conductivity and dielectric properties of solid polymer nanocomposite films: Effect of $BaTiO_3$ nanofiller. *Mater. Today Proc.* **2020**, *32*, 476–482. [CrossRef]
100. Wang, Q.; Che, J.; Wu, W.; Hu, Z.; Liu, X.; Ren, T.; Zhang, J. Contributing Factors of Dielectric Properties for Polymer Matrix Composites. *Polymers* **2023**, *15*, 590. [CrossRef]